Grating-coupled excitation of multiple surface plasmon-polariton waves

Muhammad Faryad* and Akhlesh Lakhtakia

Nanoengineered Metamaterials Group (NanoMM), Department of Engineering Science and Mechanics, Pennsylvania State University, University Park, Pennsylvania 16802-6812, USA

(Received 15 May 2011; published 28 September 2011)

The excitation of multiple surface plasmon-polariton (SPP) waves of different linear polarization states and phase speeds by a surface-relief grating formed by a metal and a rugate filter, both of finite thickness, was studied theoretically, using rigorous coupled-wave analysis. The incident plane wave can be either p or s polarized. The excitation of SPP waves is indicated by the presence of those peaks in the plots of absorptance vs the incidence angle that are independent of the thickness of the rugate filter. The absorptance peaks representing the excitation of s-polarized SPP waves are narrower than those representing p-polarized SPP waves. Two incident plane waves propagating in different directions may excite the same SPP wave. A line source could excite several SPP waves simultaneously.

DOI: 10.1103/PhysRevA.84.033852 PACS number(s): 42.25.−p, 42.70.−a

I. INTRODUCTION

Surface plasmon-polariton (SPP) waves are surface waves guided by a planar interface of a metal and a dielectric material. SPP waves find applications for sensing, imaging, and communication [1,2]. If the dielectric partnering material is isotropic and homogeneous, only one SPP wave—that too, of the p-polarization state—can be guided by the metal-dielectric interface at a given frequency [3,4]. If a periodic nonhomogeneity normal to the wave-guiding interface is introduced in the dielectric partnering material, multiple SPP waves with different polarization states, phase speeds, and spatial profiles can be guided by the metal-dielectric interface. This has recently been shown both theoretically [5–7] and experimentally [8–10]. In all of these studies, the dielectric partnering material is also locally orthorhombic.

Very recently, we have solved a canonical boundary-value problem [11] to show that multiple SPP waves can be guided even if the dielectric partnering material is isotropic—provided that material is also periodically nonhomogeneous normal to the interface. This is a very attractive result, because both partnering materials are isotropic and because the dielectric partnering material can be fabricated as a rugate filter [12–16].

The canonical boundary-value problem does not possess direct practical significance, because both partnering materials are assumed to be semi-infinite normal to the planar interface. Therefore, we set out to investigate the excitation of multiple SPP waves by the periodically corrugated interface of a metal and a rugate filter. This grating-coupled configuration [2, pp. 35–41] is popular, when the dielectric partnering material is homogeneous, because it allows the excitation of an SPP wave by a nonspecular Floquet harmonic. The interplay of the periodic nonhomogeneity of the dielectric partnering material and a periodically corrugated interface is phenomenologically rich [17,18], and should lead to the excitation of multiple SPP waves as different Floquet harmonics.

The relevant boundary-value problem was formulated using the rigorous coupled-wave analysis (RCWA) [19,20]. In this numerical technique, the constitutive parameters are expanded in terms of Fourier series with known expansion coefficients, and the electromagnetic field phasors are expanded in terms of Floquet harmonics whose coefficients are determined by substitution in the frequency-domain Maxwell curl postulates. The accuracy of the solution is conventionally held to depend only on the number of Floquet harmonics actually used in the computations [21]. The RCWA has been used to solve for scattering by a variety of surface-relief gratings [20–23], generally with both partnering materials being homogeneous.

The theoretical formulation of the boundary-value problem is provided in Sec. II and the numerical results are discussed in Sec. III. Concluding remarks are presented in Sec. IV. An $\exp(-i\omega t)$ time dependence is implicit, with ω denoting the angular frequency. The free-space wave number, the free-space wavelength, and the intrinsic impedance of free space are denoted by $k_0 = \omega\sqrt{\epsilon_0\mu_0}$, $\lambda_0 = 2\pi/k_0$, and $\eta_0 = \sqrt{\mu_0/\epsilon_0}$, respectively, with μ_0 and ϵ_0 being the permeability and permittivity of free space. Vectors are in boldface, column vectors are in boldface and enclosed within square brackets, and matrices are underlined twice and square-bracketed. The asterisk denotes the complex conjugate, the superscript T denotes the transpose, and the Cartesian unit vectors are identified as $\hat{\mathbf{u}}_x$, $\hat{\mathbf{u}}_y$, and $\hat{\mathbf{u}}_z$. The real part of a complex number ζ is denoted by $\mathrm{Re}(\zeta)$.

II. BOUNDARY-VALUE PROBLEM

A. Description

Let us consider the boundary-value problem shown schematically in Fig. 1. The regions $z < 0$ and $z > d_3$ are vacuous, the region $0 \leqslant z \leqslant d_1$ is occupied by the dielectric partnering material with relative permittivity $\epsilon_d(z)$, and the region $d_2 \leqslant z \leqslant d_3$ by the metallic partnering material with spatially uniform relative permittivity ϵ_m. The region $d_1 < z < d_2$ contains a surface-relief grating of period L along the x axis. The relative permittivity $\epsilon_g(x,z) = \epsilon_g(x \pm L, z)$ in this region is taken to be as

$$\epsilon_g(x,z) = \begin{cases} \epsilon_m - [\epsilon_m - \epsilon_d(z)]\mathcal{U}(d_2 - z - g(x)), & x \in (0, L_1), \\ \epsilon_d(z), & x \in (L_1, L), \end{cases} \tag{1}$$

*faryad@psu.edu

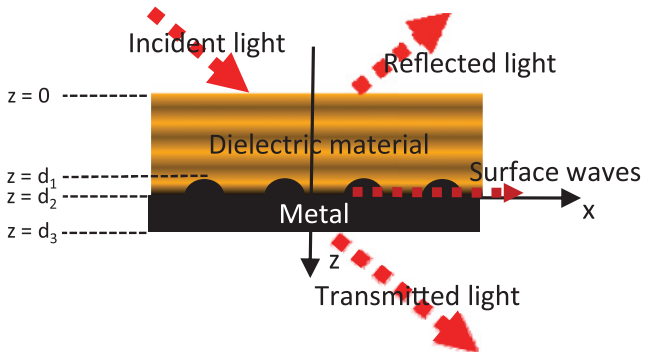

FIG. 1. (Color online) Schematic of the boundary-value problem solved using the RCWA.

for $z \in (d_1, d_2)$, with

$$g(x) = (d_2 - d_1)\sin\left(\frac{\pi x}{L_1}\right), \quad L_1 \in (0, L), \tag{2}$$

and

$$\mathcal{U}(\zeta) = \begin{cases} 1, & \zeta \geqslant 0, \\ 0, & \zeta < 0. \end{cases} \tag{3}$$

The depth of the surface-relief grating defined by Eq. (2) is $d_2 - d_1$. This particular grating shape is chosen for the ease of fabrication; however, the theoretical formulation given in the remainder of this section is independent of the shape of the surface-relief grating.

In the vacuous half-space $z \leqslant 0$, let a plane wave propagating in the xz plane at an angle θ to the z axis be incident on the structure. Hence, the incident, reflected, and transmitted

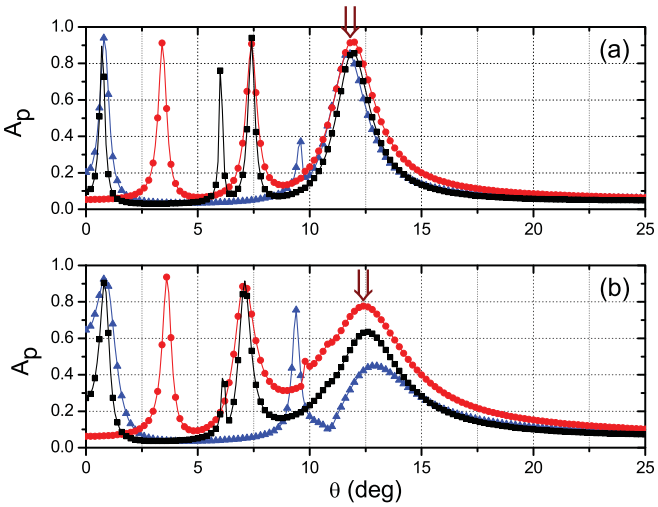

FIG. 2. (Color online) Absorptance A_p as a function of the incidence angle θ when the surface-relief grating is defined by either (a) Eq. (53) or (b) Eq. (2). Black squares represent $d_1 = 1500$ nm, red circles $d_1 = 1000$ nm, and blue triangles $d_1 = 800$ nm. The grating depth ($d_2 - d_1 = 50$ nm) and the thickness of the metallic layer ($d_3 - d_2 = 30$ nm) are the same for all cases. The vertical arrows identify SPP waves.

TABLE I. Relative wave numbers $k_x^{(n)}/k_0$ of Floquet harmonics at the θ value of the peak identified in Fig. 2 by a vertical arrow. A boldface entry signifies an SPP wave.

	$n=-2$	$n=-1$	$n=0$	$n=1$	$n=2$
$\theta = 12.5^\circ$	−2.1645	−0.9740	0.2164	**1.4069**	2.5974

field phasors may be written in terms of Floquet harmonics as follows:

$$\mathbf{E}_{\rm inc}(\mathbf{r}) = \sum_{n\in\mathbb{Z}} \left(\mathbf{s}_n a_s^{(n)} + \mathbf{p}_n^+ a_p^{(n)}\right) \exp\left[i\left(k_x^{(n)} x + k_z^{(n)} z\right)\right], \tag{4}$$
$$z \leqslant 0,$$

$$\mathbf{H}_{\rm inc}(\mathbf{r}) = \eta_0^{-1} \sum_{n\in\mathbb{Z}} \left(\mathbf{p}_n^+ a_s^{(n)} - \mathbf{s}_n a_p^{(n)}\right) \exp\left[i\left(k_x^{(n)} x + k_z^{(n)} z\right)\right], \tag{5}$$
$$z \leqslant 0,$$

$$\mathbf{E}_{\rm ref}(\mathbf{r}) = \sum_{n\in\mathbb{Z}} \left(\mathbf{s}_n r_s^{(n)} + \mathbf{p}_n^- r_p^{(n)}\right) \exp\left[i\left(k_x^{(n)} x - k_z^{(n)} z\right)\right], \tag{6}$$
$$z \leqslant 0,$$

$$\mathbf{H}_{\rm ref}(\mathbf{r}) = \eta_0^{-1} \sum_{n\in\mathbb{Z}} \left(\mathbf{p}_n^- r_s^{(n)} - \mathbf{s}_n r_p^{(n)}\right) \exp\left[i\left(k_x^{(n)} x - k_z^{(n)} z\right)\right], \tag{7}$$
$$z \leqslant 0,$$

$$\mathbf{E}_{\rm tr}(\mathbf{r}) = \sum_{n\in\mathbb{Z}} \left(\mathbf{s}_n t_s^{(n)} + \mathbf{p}_n^+ t_p^{(n)}\right) \exp\left\{i\left[k_x^{(n)} x + k_z^{(n)}(z - d_3)\right]\right\}, \tag{8}$$
$$z \geqslant d_3,$$

$$\mathbf{H}_{\rm tr}(\mathbf{r}) = \eta_0^{-1} \sum_{n\in\mathbb{Z}} \left(\mathbf{p}_n^+ t_s^{(n)} - \mathbf{s}_n t_p^{(n)}\right) \times \exp\left\{i\left[k_x^{(n)} x + k_z^{(n)}(z - d_3)\right]\right\}, \quad z \geqslant d_3, \tag{9}$$

where $k_x^{(n)} = k_0 \sin\theta + n\kappa_x$, $\kappa_x = 2\pi/L$, and

$$k_z^{(n)} = \begin{cases} +\sqrt{k_0^2 - \left(k_x^{(n)}\right)^2}, & k_0^2 > \left(k_x^{(n)}\right)^2 \\ +i\sqrt{\left(k_x^{(n)}\right)^2 - k_0^2}, & k_0^2 < \left(k_x^{(n)}\right)^2 \end{cases}. \tag{10}$$

The unit vectors

$$\mathbf{s}_n = \hat{\mathbf{u}}_y \tag{11}$$

and

$$p_n^\pm = \mp \frac{k_z^{(n)}}{k_0} \hat{\mathbf{u}}_x + \frac{k_x^{(n)}}{k_0} \hat{\mathbf{u}}_z \tag{12}$$

represent the s- and p-polarization states, respectively.

B. Coupled ordinary differential equations

The relative permittivity in the region $0 \leqslant z \leqslant d_3$ can be expanded as a Fourier series with respect to x, viz.,

$$\epsilon(x,z) = \sum_{n\in\mathbb{Z}} \epsilon^{(n)}(z)\exp(in\kappa_x x)\,, \quad z\in[0,d_3]\,, \tag{13}$$

where

$$\epsilon^{(0)}(z) = \begin{cases} \epsilon_d(z)\,, & z\in[0,d_1]\,, \\ \frac{1}{L}\int_0^L \epsilon_g(x,z)dx\,, & z\in(d_1,d_2)\,, \\ \epsilon_m\,, & z\in[d_2,d_3]\,, \end{cases} \tag{14}$$

and

$$\epsilon^{(n)}(z) = \begin{cases} \frac{1}{L}\int_0^L \epsilon_g(x,z)\exp(-in\kappa_x x)dx\,, & z\in[d_1,d_2] \\ 0\,, & \text{otherwise} \end{cases} ;\, \forall\, n\neq 0\,. \tag{15}$$

The field phasors may be written in the region $0 \leqslant z \leqslant d_3$ in terms of Floquet harmonics as

$$\mathbf{E}(\mathbf{r}) = \sum_{n\in\mathbb{Z}} \mathbf{E}^{(n)}(z)\exp\left(ik_x^{(n)}x\right),$$
$$\mathbf{H}(\mathbf{r}) = \sum_{n\in\mathbb{Z}} \mathbf{H}^{(n)}(z)\exp\left(ik_x^{(n)}x\right), \quad z\in[0,d_3]\,, \tag{16}$$

with unknown functions $\mathbf{E}^{(n)}(z) = E_x^{(n)}(z)\hat{\mathbf{u}}_x + E_y^{(n)}(z)\hat{\mathbf{u}}_y + E_z^{(n)}(z)\hat{\mathbf{u}}_z$ and $\mathbf{H}^{(n)}(z) = H_x^{(n)}(z)\hat{\mathbf{u}}_x + H_y^{(n)}(z)\hat{\mathbf{u}}_y + H_z^{(n)}(z)\hat{\mathbf{u}}_z$.

Substitution of Eqs. (13) and (16) in the frequency-domain Maxwell curl postulates results in a system of four ordinary differential equations and two algebraic equations as follows:

$$\frac{d}{dz}E_x^{(n)}(z) - ik_x^{(n)}E_z^{(n)}(z) = ik_0\eta_0 H_y^{(n)}(z)\,, \tag{17}$$

$$\frac{d}{dz}E_y^{(n)}(z) = -ik_0\eta_0 H_x^{(n)}(z)\,, \tag{18}$$

$$k_x^{(n)}E_y^{(n)}(z) = k_0\eta_0 H_z^{(n)}(z)\,, \tag{19}$$

$$\frac{d}{dz}H_x^{(n)}(z) - ik_x^{(n)}H_z^{(n)}(z) = -\frac{ik_0}{\eta_0}\sum_{m\in\mathbb{Z}}\epsilon^{(n-m)}(z)E_y^{(m)}(z)\,, \tag{20}$$

$$\frac{d}{dz}H_y^{(n)}(z) = \frac{ik_0}{\eta_0}\sum_{m\in\mathbb{Z}}\epsilon^{(n-m)}(z)E_x^{(m)}(z)\,, \tag{21}$$

$$k_x^{(n)}H_y^{(n)}(z) = -\frac{k_0}{\eta_0}\sum_{m\in\mathbb{Z}}\epsilon^{(n-m)}(z)E_z^{(m)}(z)\,. \tag{22}$$

Equations (17)–(22) hold $\forall\, z\in(0,d_3)$ and $\forall\, n\in\mathbb{Z}$. These equations can be recast into an infinite system of coupled first-order ordinary differential equations. This system can not be implemented on a digital computer. Therefore, we restrict $|n|\leqslant N_t$ and then define the column $(2N_t+1)$ vectors

$$[\mathbf{X}_\sigma(z)] = \left[X_\sigma^{(-N_t)}(z), X_\sigma^{(-N_t)}(z), \ldots, X_\sigma^{(0)}(z), \ldots, X_\sigma^{(N_t-1)}(z), X_\sigma^{(N_t)}(z)\right]^T, \tag{23}$$

for $X\in\{E,H\}$ and $\sigma\in\{x,y,z\}$. Similarly, we define $(2N_t+1)\times(2N_t+1)$-matrices

$$\left[\underline{\underline{K}}_x\right] = \mathrm{diag}\left[k_x^{(n)}\right], \quad \left[\underline{\underline{\epsilon}}(z)\right] = \left[\epsilon^{(n-m)}(z)\right], \tag{24}$$

where $\mathrm{diag}[k_x^{(n)}]$ is a diagonal matrix.

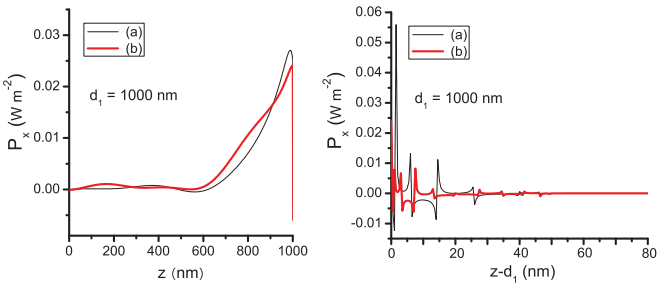

FIG. 3. (Color online) Variation of the x component of the time-averaged Poynting vector $\mathbf{P}(x,z)$ along the z axis in the regions (left) $0<z<d_1$ and (right) $d_1<z<d_3$ at $x=0.75L$ for $\theta=12.5^\circ$, when the surface-relief grating is defined by either (a) Eq. (53) or (b) Eq. (2) and the incident plane wave is p polarized. Other parameters are the same as for Fig. 2.

Equations (19) and (22) yield

$$[\mathbf{E}_z(z)] = -\frac{\eta_0}{k_0}\left[\underline{\underline{\epsilon}}(z)\right]^{-1}\cdot\left[\underline{\underline{K}}_x\right]\cdot[\mathbf{H}_y(z)] \tag{25}$$

and

$$[\mathbf{H}_z(z)] = \frac{1}{\eta_0 k_0}\left[\underline{\underline{K}}_x\right]\cdot[\mathbf{E}_y(z)], \tag{26}$$

the use of which in Eqs. (17), (18), (20), and (21) eliminates $E_z^{(n)}$ and $H_z^{(n)}\,\forall\, n\in\mathbb{Z}$, and gives the matrix ordinary differential equation

$$\frac{d}{dz}[\mathbf{f}(z)] = i\left[\underline{\underline{P}}(z)\right]\cdot[\mathbf{f}(z)]\,, \quad z\in(0,d_3)\,, \tag{27}$$

where the column vector $[\mathbf{f}(z)]$ with $4(2N_t+1)$ components is defined as

$$[\mathbf{f}(z)] = [[\mathbf{E}_x(z)]^T, [\mathbf{E}_y(z)]^T, \eta_0[\mathbf{H}_x(z)]^T, \eta_0[\mathbf{H}_y(z)]^T]^T \tag{28}$$

and the $4(2N_t+1)\times 4(2N_t+1)$-matrix $[\underline{\underline{P}}(z)]$ is given by

$$\left[\underline{\underline{P}}(z)\right] = \begin{bmatrix} [\underline{0}] & [\underline{0}] & [\underline{0}] & \left[\underline{\underline{P}}_{14}(z)\right] \\ [\underline{0}] & [\underline{0}] & -k_0\left[\underline{I}\right] & [\underline{0}] \\ [\underline{0}] & \left[\underline{\underline{P}}_{32}(z)\right] & [\underline{0}] & [\underline{0}] \\ \left[\underline{\underline{P}}_{41}(z)\right] & [\underline{0}] & [\underline{0}] & [\underline{0}] \end{bmatrix}. \tag{29}$$

Whereas $[\underline{0}]$ is the $(2N_t+1)\times(2N_t+1)$ null matrix and $[\underline{I}]$ is the $(2N_t+1)\times(2N_t+1)$ identity matrix, the three non-null submatrices on the right side of Eq. (29) are as follows:

$$\left[\underline{\underline{P}}_{14}(z)\right] = k_0[\underline{I}] - \frac{1}{k_0}\left[\underline{\underline{K}}_x\right]\cdot\left[\underline{\underline{\epsilon}}(z)\right]^{-1}\cdot\left[\underline{\underline{K}}_x\right], \tag{30}$$

$$\left[\underline{\underline{P}}_{32}(z)\right] = \frac{1}{k_0}\left[\underline{\underline{K}}_x\right]^2 - k_0\left[\underline{\underline{\epsilon}}(z)\right], \tag{31}$$

$$\left[\underline{\underline{P}}_{41}(z)\right] = k_0\left[\underline{\underline{\epsilon}}(z)\right]. \tag{32}$$

C. Solution algorithm

The column vectors $[\mathbf{f}(0)]$ and $[\mathbf{f}(d_3)]$ can be written using Eqs. (4)–(9) as

$$[\mathbf{f}(0)] = \begin{bmatrix} \left[\underline{\underline{Y}}_e^+\right] & \left[\underline{\underline{Y}}_e^-\right] \\ \left[\underline{\underline{Y}}_h^+\right] & \left[\underline{\underline{Y}}_h^-\right] \end{bmatrix}\cdot\begin{bmatrix}[\mathbf{A}] \\ [\mathbf{R}]\end{bmatrix}, \quad [\mathbf{f}(d_3)] = \begin{bmatrix} \left[\underline{\underline{Y}}_e^+\right] \\ \left[\underline{\underline{Y}}_h^+\right] \end{bmatrix}\cdot[\mathbf{T}]\,, \tag{33}$$

TABLE II. Relative wave numbers κ/k_0 of possible SPP waves obtained by the solution of the canonical boundary-value problem [11] for $\Omega = \lambda_0$. Other parameters are provided in the beginning of Sec. III B. If κ represents an SPP wave propagating in the $\hat{\mathbf{u}}_x$ direction, $-\kappa$ represents an SPP wave propagating in the $-\hat{\mathbf{u}}_x$ direction.

Polarization	Relative wave numbers				
s	$1.48639 + 0.00132i$	$1.7324 + 0.0014i$[a]			
p	$1.36479 + 0.00169i$	$1.61782 + 0.00548i$	$1.87437 + 0.00998i$	$2.06995 + 0.01526i$	$2.21456 + 0.00246i$

[a]This solution had been missed when solutions for Fig. 1 of Ref. [11] were numerically searched.

where

$$[\mathbf{A}] = \left[a_s^{(-N_t)}, a_s^{(-N_t+1)}, \ldots, a_s^{(0)}, \ldots, a_s^{(N_t-1)}, a_s^{(N_t)}, a_p^{(-N_t)}, a_p^{(-N_t+1)}, \ldots, a_p^{(0)}, \ldots, a_p^{(N_t-1)}, a_p^{(N_t)}\right]^T , \tag{34}$$

$$[\mathbf{R}] = \left[r_s^{(-N_t)}, r_s^{(-N_t+1)}, \ldots, r_s^{(0)}, \ldots, r_s^{(N_t-1)}, r_s^{(N_t)}, r_p^{(-N_t)}, r_p^{(-N_t+1)}, \ldots, r_p^{(0)}, \ldots, r_p^{(N_t-1)}, r_p^{(N_t)}\right]^T , \tag{35}$$

$$[\mathbf{T}] = \left[t_s^{(-N_t)}, t_s^{(-N_t+1)}, \ldots, t_s^{(0)}, \ldots, t_s^{(N_t-1)}, t_s^{(N_t)}, t_p^{(-N_t)}, t_p^{(-N_t+1)}, \ldots, t_p^{(0)}, \ldots, t_p^{(N_t-1)}, t_p^{(N_t)}\right]^T , \tag{36}$$

and the nonzero entries of $(4N_t + 2) \times (4N_t + 2)$-matrices $[\underline{\underline{Y}}_{e,h}^{\pm}]$ are as follows:

$$(Y_e^{\pm})_{nm} = 1 , \quad n = m + 2N_t + 1 , \tag{37}$$

$$(Y_e^{\pm})_{nm} = \mp \frac{k_z^{(n)}}{k_0} , \quad n = m - 2N_t - 1 , \tag{38}$$

$$(Y_h^{\pm})_{nm} = \mp \frac{k_z^{(n)}}{k_0} , \quad n = m \in [1, 2N_t + 1] , \tag{39}$$

$$(Y_h^{\pm})_{nm} = -1 , \quad n = m \in [2N_t + 2, 4N_t + 2] . \tag{40}$$

In order to devise a stable algorithm [20,21,23,24], the region $0 \leqslant z \leqslant d_1$ is divided into N_d slices and the region $d_1 < z < d_2$ into N_g slices, but the region $d_2 \leqslant z \leqslant d_3$ is kept as just one slice. So, there are $N_d + N_g + 1$ slices and $N_d + N_g + 2$ interfaces. In the jth slice, $j \in [1, N_d + N_g + 1]$, bounded by the planes $z = z_{j-1}$ and $z = z_j$, we approximate

$$\left[\underline{\underline{P}}(z)\right] = \left[\underline{\underline{P}}\right]_j = \left[\underline{\underline{P}}\left(\frac{z_j + z_{j-1}}{2}\right)\right] , \quad z \in (z_j, z_{j-1}) , \tag{41}$$

so that Eq. (27) yields

$$[\mathbf{f}(z_{j-1})] = \left[\underline{\underline{G}}\right]_j \cdot \exp\left\{ - i\Delta_j \left[\underline{\underline{D}}\right]_j \right\} \cdot \left[\underline{\underline{G}}\right]_j^{-1} \cdot [\mathbf{f}(z_j)] , \tag{42}$$

where $\Delta_j = z_j - z_{j-1}$, $[\underline{\underline{G}}]_j$ is a square matrix comprising the eigenvectors of $[\underline{\underline{P}}]_j$ as its columns, and the diagonal matrix $[\underline{\underline{D}}]_j$ contains the eigenvalues of $[\underline{\underline{P}}]_j$ in the same order.

Let us define auxiliary column vectors $[\mathbf{T}]_j$ and auxiliary transmission matrices $[\underline{\underline{Z}}]_j$ by the relation [23]

$$[\mathbf{f}(z_j)] = \left[\underline{\underline{Z}}\right]_j \cdot [\mathbf{T}]_j , \quad j \in [0, N_d + N_g + 1] , \tag{43}$$

where $z_0 = 0$,

$$[\mathbf{T}]_{N_d+N_g+1} = [\mathbf{T}] , \quad \text{and} \quad \left[\underline{\underline{Z}}\right]_{N_d+N_g+1} = \begin{bmatrix} \left[\underline{\underline{Y}}_e^{+}\right] \\ \left[\underline{\underline{Y}}_h^{+}\right] \end{bmatrix} . \tag{44}$$

To find $[\mathbf{T}]_j$ and $[\underline{\underline{Z}}]_j$ for $j \in [0, N_d + N_g]$, we substitute Eq. (43) in Eq. (42), which results in the relation

$$\left[\underline{\underline{Z}}\right]_{j-1} \cdot [\mathbf{T}]_{j-1} = \left[\underline{\underline{G}}\right]_j \cdot \begin{bmatrix} e^{-i\Delta_j [\underline{\underline{D}}]_j^u} & 0 \\ 0 & e^{-i\Delta_j \left[\underline{\underline{D}}\right]_j^l} \end{bmatrix} \cdot \left[\underline{\underline{G}}\right]_j^{-1} \cdot \left[\underline{\underline{Z}}\right]_j \cdot [\mathbf{T}]_j , \quad j \in [1, N_d + N_g + 1] , \tag{45}$$

where $[\underline{\underline{D}}]_j^u$ and $[\underline{\underline{D}}]_j^l$ are the upper and lower diagonal submatrices of $[\underline{\underline{D}}]_j$, respectively, when the eigenvalues are arranged in decreasing order of the imaginary part.

Since $[\mathbf{T}]_j$ and $[\underline{\underline{Z}}]_j$ cannot be determined simultaneously from Eq. (45), let us define [23]

$$[\mathbf{T}]_{j-1} = \exp\left\{ - i\Delta_j \left[\underline{\underline{D}}\right]_j^u \right\} \cdot \left[\underline{\underline{W}}\right]_j^u \cdot [\mathbf{T}]_j , \tag{46}$$

where the square matrix $[\underline{\underline{W}}]_j^u$ and its counterpart $[\underline{\underline{W}}]_j^l$ are defined via

$$\begin{bmatrix} \left[\underline{\underline{W}}\right]_j^u \\ \left[\underline{\underline{W}}\right]_j^l \end{bmatrix} = \left[\underline{\underline{G}}\right]_j^{-1} \cdot \left[\underline{\underline{Z}}\right]_j . \tag{47}$$

Substitution of Eq. (46) in Eq. (45) results in the relation

$$\left[\underline{\underline{Z}}\right]_{j-1} = \left[\underline{\underline{G}}\right]_j \cdot \begin{bmatrix} \left[\underline{\underline{I}}\right] \\ \exp\left\{-i\Delta_j \left[\underline{\underline{D}}\right]_j^l\right\} \cdot \left[\underline{\underline{W}}\right]_j^l \cdot \left\{\left[\underline{\underline{W}}\right]_j^u\right\}^{-1} \cdot \exp\left\{i\Delta_j \left[\underline{\underline{D}}\right]_j^u\right\} \end{bmatrix} , \quad j \in [1, N_d + N_g + 1] . \tag{48}$$

From Eqs. (47) and (48), we find $[\underline{\underline{Z}}]_0$ in terms of $[\underline{\underline{Z}}]_{N_d+N_g+1}$. After partitioning

$$\left[\underline{\underline{Z}}\right]_0 = \begin{bmatrix} \left[\underline{\underline{Z}}\right]_0^u \\ \left[\underline{\underline{Z}}\right]_0^l \end{bmatrix} , \tag{49}$$

and using Eqs. (33) and (43), $[\mathbf{R}]$ and $[\mathbf{T}]_0$ are found as follows:

$$\begin{bmatrix} [\mathbf{T}]_0 \\ [\mathbf{R}] \end{bmatrix} = \begin{bmatrix} \left[\underline{\underline{Z}}\right]_0^u & -\left[\underline{\underline{Y}}_e^{-}\right] \\ \left[\underline{\underline{Z}}\right]_0^l & -\left[\underline{\underline{Y}}_h^{-}\right] \end{bmatrix}^{-1} \cdot \begin{bmatrix} \left[\underline{\underline{Y}}_e^{+}\right] \\ \left[\underline{\underline{Y}}_h^{+}\right] \end{bmatrix} \cdot [\mathbf{A}] . \tag{50}$$

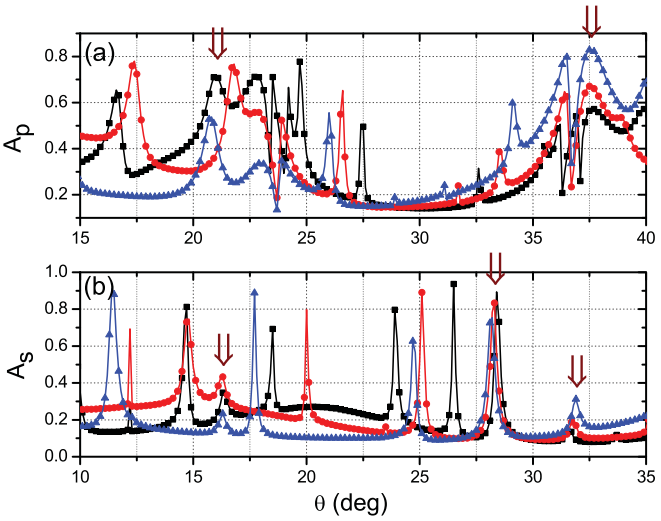

FIG. 4. (Color online) Absorptances (a) A_p and (b) A_s as functions of the incidence angle θ, when the surface-relief grating is defined by Eq. (2) with $L_1 = 0.5L$, $\lambda_0 = 633$ nm, $\Omega = \lambda_0$, and $L = \lambda_0$. Black squares are for $d_1 = 6\Omega$, red circles for $d_1 = 5\Omega$, and blue triangles for $d_1 = 4\Omega$. The grating depth ($d_2 - d_1 = 50$ nm) and the thickness of the metallic layer ($d_3 - d_2 = 30$ nm) are the same for all plots. Each vertical arrow identifies an SPP wave.

Equation (50) is obtained by enforcing the usual boundary conditions across the plane $z = 0$. After $[\mathbf{T}]_0$ is known, $[\mathbf{T}] = [\mathbf{T}]_{N_d+N_g+1}$ is found by reversing the sense of iterations in Eq. (46).

III. NUMERICAL RESULTS AND DISCUSSION

A. Homogeneous dielectric partnering material

Let us begin with the dielectric partnering material being homogeneous, i.e., $\epsilon_d(z)$ is independent of z. This case has been numerically illustrated by Homola [[2], p. 38] and we adopted the same parameters: $\lambda_0 = 800$ nm, $\epsilon_d = 1.766$ (water), $\epsilon_m = -25 + 1.44i$ (gold), and $L = 672$ nm. The incident plane wave is p polarized ($a_p^{(n)} = \delta_{n0}$ V m^{-1} and $a_s^{(n)} \equiv 0\ \forall\, n \in \mathbb{Z}$), and the quantity of importance is the absorptance

$$A_p = 1 - \sum_{n=-N_t}^{N_t} \left(\left|r_s^{(n)}\right|^2 + \left|r_p^{(n)}\right|^2 + \left|t_s^{(n)}\right|^2 + \left|t_p^{(n)}\right|^2\right) \times \mathrm{Re}\left(k_z^{(n)}/k_z^{(0)}\right), \tag{51}$$

TABLE III. Relative wave numbers $k_x^{(n)}/k_0$ of Floquet harmonics at the θ values of the peaks identified in Fig. 4 by vertical arrows when $\Omega = \lambda_0$ and $L = \lambda_0$. Boldface entries signify SPP waves.

	$n=-2$	$n=-1$	$n=0$	$n=1$	$n=2$
$\theta = 16.3^\circ$	**−1.7210**	−0.7210	0.2790	1.2790	2.2790
$\theta = 21.0^\circ$	−1.6416	−0.6416	0.3584	**1.3584**	2.3584
$\theta = 28.4^\circ$	−1.5244	−0.5244	0.4756	**1.4756**	2.4756
$\theta = 31.6^\circ$	**−1.4760**	−0.4760	0.5240	1.5240	2.5240
$\theta = 37.7^\circ$	−1.3885	−0.3885	0.6115	**1.6115**	2.6115

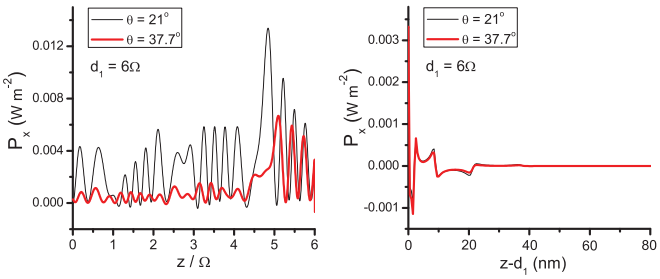

FIG. 5. (Color online) Variation of the x component of the time-averaged Poynting vector $\mathbf{P}(x,z)$ along the z axis in the regions (left) $0 < z < d_1$ and (right) $d_1 < z < d_3$ at $x = 0.75L$, when the surface-relief grating is defined by Eq. (2). The grating period $L = \lambda_0$ and the incident plane wave is p polarized. Other parameters are the same as for Fig. 4.

which simplifies to

$$A_p = 1 - \sum_{n=-N_t}^{N_t} \left(\left|r_p^{(n)}\right|^2 + \left|t_p^{(n)}\right|^2\right)\mathrm{Re}\left(k_z^{(n)}/k_z^{(0)}\right), \tag{52}$$

because all materials are isotropic.

Figure 2(a) shows the variation of A_p vs the incidence angle θ for a sinusoidal surface-relief grating defined by [2]

$$g(x) = \frac{1}{2}(d_2 - d_1)\left[1 + \sin\left(\frac{2\pi x}{L}\right)\right] \tag{53}$$

instead of Eq. (2), and Fig. 2(b) shows the same for the surface-relief grating defined by Eq. (2) with $L_1 = 0.5L$. For computational purposes, we set $N_d = 1$, $N_g = 50$, and $N_t = 10$, after ascertaining that all nonzero reflectances $|r_p^{(n)}|^2\mathrm{Re}(k_z^{(n)}/k_z^{(0)})$ and transmittances $|t_p^{(n)}|^2\mathrm{Re}(k_z^{(n)}/k_z^{(0)})$ converged within $\pm 0.5\%$ for all $n \in [-N_t, N_t]$.

Each figure shows plots of A_p vs θ for three different values of the thickness d_1, in order to distinguish [25] between

(i) surface waves [11], which must be independent of d_1 for sufficiently large values of that parameter, and

(ii) waveguide modes [26,27], which must depend on d_1,

as has been shown elsewhere [28,29]. In both figures, an absorptance peak at $\theta \simeq 12.5^\circ$ for all three values of d_1 indicates the excitation of an SPP wave. Parenthetically, let us note here that an SPP wave is a solution of a canonical boundary-value problem involving the planar interface of two semi-infinite half spaces, one of which is occupied by a metal and the other by a dielectric material; but, as the canonical boundary-value problem cannot be implemented practically,

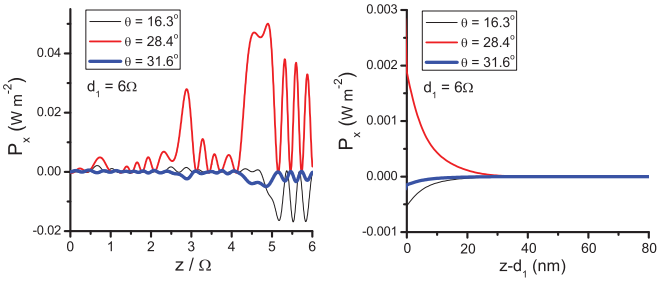

FIG. 6. (Color online) Same as Fig. 5 except that the incident plane wave is s polarized.

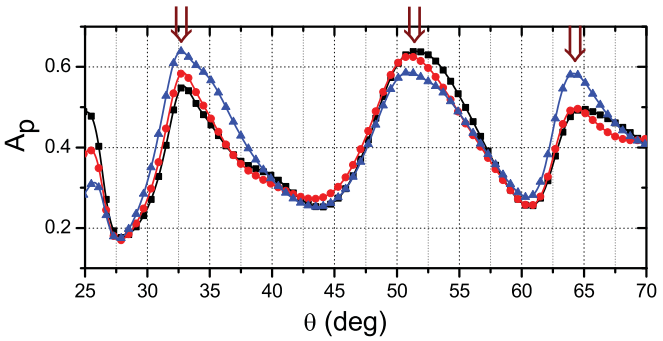

FIG. 7. (Color online) Absorptance A_p as a function of the incidence angle θ, when the surface-relief grating is defined by Eq. (2) with $L_1 = 0.5L$, $\lambda_0 = 633$ nm, $\Omega = \lambda_0$, and $L = 0.75\lambda_0$. Black squares are for $d_1 = 6\Omega$, red circles for $d_1 = 5\Omega$, and blue triangles for $d_1 = 4\Omega$. The grating depth ($d_2 - d_1 = 50$ nm) and the thickness of the metallic layer ($d_3 - d_2 = 30$ nm) are the same for all plots. Each vertical arrow identifies an SPP wave.

both materials must be present as sufficiently thick layers in a real situation so that the SPP wave decays appreciably through the thickness of each layer.

The relative wave numbers $k_x^{(n)}/k_0$ of a few Floquet harmonics at $\theta = 12.5^\circ$ are given in Table I. The solution of the canonical boundary-value problem [2] (when both partnering materials are semi-infinite along the z axis and their interface is planar) shows that the relative wave number κ/k_0 of the SPP wave that can be guided by the planar gold-water interface is

$$\kappa/k_0 = \sqrt{\epsilon_d\epsilon_m/(\epsilon_d+\epsilon_m)} = 1.3784 + 0.0030i\,. \quad (54)$$

A comparison of Table I and Eq. (54) confirms that an SPP wave is excited at $\theta = 12.5^\circ$ as the Floquet harmonic of order $n = 1$. The spatial profiles of the x component of the time-averaged Poynting vector

$$\mathbf{P}(x,z) = \tfrac{1}{2}\mathrm{Re}[\mathbf{E}(x,z)\times\mathbf{H}^*(x,z)] \quad (55)$$

along the z axis for $x = 0.75L$ for the p-polarized incident plane wave at $\theta = 12.5^\circ$ (the θ value of the peak identified in Fig. 2 by a vertical arrow), presented in Fig. 3, also indicate that p-polarized SPP waves are indeed excited for both types of the surface-relief grating because P_x decays quickly away from the interface $z = d_1$.

We note that the absorptance peak in Fig. 2(b) is not only wider than in Fig. 2(a), but also of lower magnitude, which points out the critical importance of the shape function $g(x)$ of the surface-relief grating. The incidence angle θ determined by Homola [2, p. 38] is approximately 11°, the small difference between his and our results being (i) due to the different methods of computation and (ii) the fact that, while Homola had semi-infinite dielectric and metallic partnering materials, we have the two of finite thickness.

TABLE IV. Relative wave numbers $k_x^{(n)}/k_0$ of Floquet harmonics at the θ values of the peaks identified in Fig. 7 by vertical arrows when $\Omega = \lambda_0$ and $L = 0.75\lambda_0$. Boldface entries signify SPP waves.

	$n=-2$	$n=-1$	$n=0$	$n=1$	$n=2$
$\theta = 32.5^\circ$	−2.1294	−0.7960	0.5373	**1.8760**	3.2040
$\theta = 50.9^\circ$	−1.8906	−0.5573	0.7760	**2.1094**	3.4427
$\theta = 64.2^\circ$	−1.7664	−0.4330	0.9003	**2.2336**	3.5670

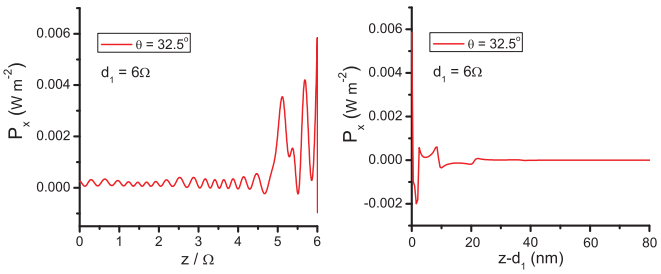

FIG. 8. (Color online) Variation of the x component of the time-averaged Poynting vector $\mathbf{P}(x,z)$ along the z axis in the regions (left) $0 < z < d_1$ and (right) $d_1 < z < d_3$ at $x = 0.75L$, when the surface-relief grating is defined by Eq. (2) and the incident plane wave is p polarized. The grating period $L = 0.75\lambda_0$, $\Omega = \lambda_0$, and $d_1 = 6\Omega$.

B. Periodically nonhomogeneous dielectric partnering material

Now let us move on to the excitation of *multiple* SPP waves by a surface-relief grating where the dielectric partnering material has a periodic nonhomogeneity normal to the mean metal-dielectric interface:

$$\epsilon_d(z) = \left[\left(\frac{n_b+n_a}{2}\right) + \left(\frac{n_b-n_a}{2}\right)\sin\left(\pi\frac{d_2-z}{\Omega}\right)\right]^2, \quad z > 0\,, \quad (56)$$

where 2Ω is the period. We chose $n_a = 1.45$ and $n_b = 2.32$ from an example provided by Baumeister [[30], Sec. 5.3.3.2]. For all calculations reported in the remainder of this paper, we chose the metal to be bulk aluminum ($\epsilon_{\mathrm{met}} = -56 + 21i$) and the free-space wavelength $\lambda_0 = 633$ nm. The surface-relief grating is defined by Eq. (2) with $L_1 = 0.5L$. We fixed $N_t = 8$ after ascertaining that the absorptances for $N_t = 8$ converged to within ±1% of the absorptances calculated with $N_t = 9$. The grating depth $d_2 - d_1 = 50$ nm and the thickness $d_3 - d_2 = 30$ nm were also fixed, as their variations would not qualitatively affect the excitation of multiple SPP waves. Numerical results for $\Omega = \lambda_0$ and $\Omega = 1.5\lambda_0$ are now presented.

1. $\Omega = \lambda_0$

Let us commence with $\Omega = \lambda_0$. The solution of the corresponding canonical boundary-value problem [11,31] (when both the rugate filter and the metal are semi-infinite in thickness and their interface is planar) results in five p-polarized and two

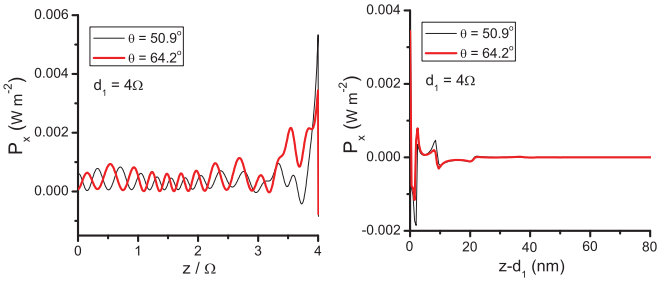

FIG. 9. (Color online) Same as Fig. 8 except that $d_1 = 4\Omega$.

TABLE V. Same as Table II except for $\Omega = 1.5\lambda_0$.

Polarization	Relative wave numbers			
s	$1.4363 + 0.00025i$[a]	$1.61507 + 0.00114i$	$1.78735 + 0.00078i$	$1.9512 + 0.00037i$[a]
p	$1.40725 + 0.00052i$	$1.54121 + 0.00374i$	$1.71484 + 0.0049i$	$1.88541 + 0.00739i$
	$2.11513 + 0.0045i$	$2.02159 + 0.01301i$		

[a]These solutions had been missed when solutions for Fig. 1 of Ref. [11] were numerically searched.

s-polarized SPP waves, the relative wave numbers κ/k_0 being provided in Table II. We used the solution of the canonical boundary-value problem as a guide to choose the grating period L and as a reference for the relative wave numbers of SPP waves. To analyze the excitation of s-polarized SPP waves in the grating-coupled configuration, we calculated the absorptance

$$A_s = 1 - \sum_{n=-N_t}^{n=N_t} \left(\left|r_s^{(n)}\right|^2 + \left|t_s^{(n)}\right|^2\right)\mathrm{Re}\left(k_z^{(n)}/k_z^{(0)}\right) \qquad (57)$$

for $a_s^{(n)} = \delta_{n0}$ V m^{-1} and $a_p^{(n)} \equiv 0\ \forall\, n \in \mathbb{Z}$. Both A_p and A_s were calculated as functions of θ for $d_1 \in \{4\Omega, 5\Omega, 6\Omega\}$, with N_g and N_d selected to have slices of thickness 2 nm in the region $0 \leqslant z \leqslant d_1$ but 1 nm in the region $d_1 < z < d_2$.

For all three values of d_1, a peak is present at $\theta = 37.7^\circ$ in the plots of A_p vs θ in Fig. 4(a). The relative wave numbers $k_x^{(n)}/k_0$ of several Floquet harmonics at this incidence angle are given in Table III. At $\theta = 37.7^\circ$, $k_x^{(1)}/k_0 = 1.6115$ is close to $\mathrm{Re}(\kappa/k_0) = 1.61782$, where κ/k_0 is the relative wave number of a p-polarized SPP wave in the canonical boundary-value problem as provided in Table II. Thus, this A_p peak represents the excitation of a p-polarized SPP wave as a Floquet harmonic of order $n = 1$. In order to confirm this conclusion, we plotted the spatial profile of $P_x(0.75L, z)$ in Fig. 5 for $\theta = 37.7^\circ$. Indeed, P_x decays quickly away from the plane $z = d_1$ in the region containing metal, and it also decays—periodically, according to the Floquet–Lyapunov theorem [32]—inside the rugate filter away from the same interface, thereby providing confirmation.

For the A_p peak at $\theta \simeq 21^\circ$, the angular location changes slightly with the change in the value of d_1. However, this peak also represents the excitation of a p-polarized SPP wave because (i) $k_x^{(1)}/k_0 = 1.3584$ (Table III) is close to $\mathrm{Re}(\kappa/k_0) = 1.36479$ (Table II), and (ii) the spatial profile of $P_x(0.75L, z)$ provided in Fig. 5 is also indicative of a surface wave guided by the metal–rugate-filter interface. The reason for the change in the θ value of the A_p peak is the weak localization of this SPP wave in the region $z < d_1$ (see the left panel in Fig. 5 for $\theta = 21^\circ$). However, for a sufficiently large value of d_1, the peak should be independent of the value of d_1.

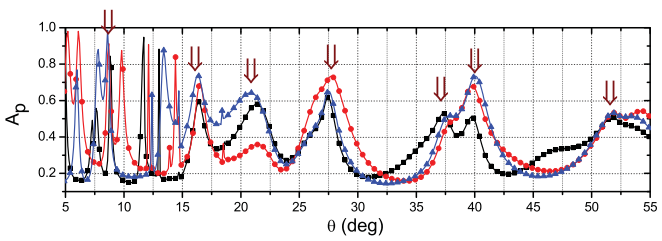

FIG. 10. (Color online) Absorptance A_p as a function of the incidence angle θ, when the surface-relief grating is defined by Eq. (2) with $L_1 = 0.5L$, $\lambda_0 = 633$ nm, $\Omega = 1.5\lambda_0$, and $L = 0.8\lambda_0$. Black squares are for $d_1 = 6\Omega$, red circles for $d_1 = 5\Omega$, and blue triangles for $d_1 = 4\Omega$. The grating depth ($d_2 - d_1 = 50$ nm) and the width of the metallic layer ($d_3 - d_2 = 30$ nm) are the same for all the plots. Each vertical arrow indicates an SPP wave.

Three A_s peaks are present at $\theta \simeq 16.3^\circ$, 28.4°, and 31.6° in the plots of A_s vs θ, for all three values of d_1 in Fig. 4(b). The relative wave numbers of Floquet harmonics at these values of the incidence angle are also provided in Table III. At $\theta = 16.3^\circ$, an s-polarized SPP wave is excited as a Floquet harmonic of order $n = -2$ because $k_x^{(-2)}/k_0 = -1.7210$ (Table III) is close to $\mathrm{Re}(\kappa/k_0) = -1.7324$ (Table II). The spatial profile of $P_x(0.75L, z)$ given in Fig. 6 for $\theta = 16.3^\circ$ also confirms this conclusion. Let us also note that the s-polarized SPP wave is propagating in the $-\hat{\mathbf{u}}_x$ direction because it is excited as a Floquet harmonic of a negative order.

The A_s peak at $\theta = 28.4^\circ$ represents the excitation of an s-polarized SPP wave, as a Floquet harmonic of order $n = 1$, because (i) $k_x^{(1)}/k_0 = 1.4756$ (Table III) is close to $\mathrm{Re}(\kappa/k_0) = 1.48639$ (Table II), and (ii) the spatial profile of $P_x(0.75L, z)$ provided in Fig. 6 shows that an s-polarized SPP wave is guided by the interface $z = d_1$ in the $+\hat{\mathbf{u}}_x$ direction. Coincidently, the A_s peak at $\theta = 31.6^\circ$ represents the excitation of the same s-polarized SPP wave but as a Floquet harmonic of order $n = -2$ because $k_x^{(-2)}/k_0 = -1.4760$ (Table III) is close to $\mathrm{Re}(\kappa/k_0) = -1.48639$ (Table II). This is also evident from the comparison of the spatial profiles given in Fig. 6 for $\theta = 28.4^\circ$ and 31.6°. Although the two spatial profiles are mirror images of each other, the excitation of the s-polarized SPP wave at $\theta = 31.6^\circ$ is not very efficient because it is excited as a Floquet harmonic of a higher order ($|n| = 2$).

Since not all possible p-polarized SPP waves (predicted from the solution of the canonical boundary-value problem)

TABLE VI. Relative wave numbers $k_x^{(n)}/k_0$ of Floquet harmonics at the θ values of the peaks identified in Fig. 10 by vertical arrows when $\Omega = 1.5\lambda_0$ and $L = 0.8\lambda_0$. Boldface entries signify SPP waves.

	$n = -2$	$n = -1$	$n = 0$	$n = 1$	$n = 2$
$\theta = 8.8^\circ$	−2.3470	−1.0970	0.1530	**1.4030**	2.6530
$\theta = 16.3^\circ$	−2.2193	−0.9693	0.2807	**1.5307**	2.7807
$\theta = 20.8^\circ$	**−2.1416**	−0.8916	0.3584	1.6084	2.8584
$\theta = 27.5^\circ$	−2.0382	−0.7882	0.4618	**1.7118**	2.9618
$\theta = 37.3^\circ$	**−1.8940**	−0.6440	0.6060	1.8560	3.1060
$\theta = 40^\circ$	−1.8572	−0.6072	0.6428	**1.8928**	3.1428
$\theta = 51.8^\circ$	−1.7141	−0.4641	0.7859	**2.0359**	3.2859

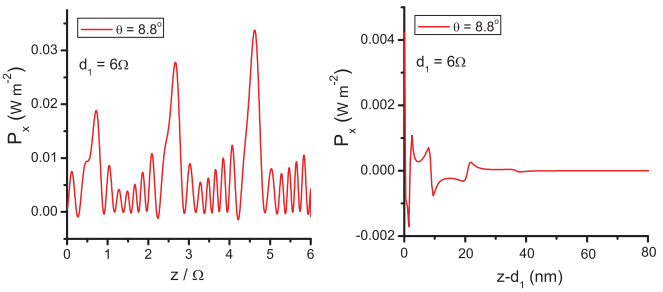

FIG. 11. (Color online) Variation of the x component of the time-averaged Poynting vector $\mathbf{P}(x,z)$ along the z axis in the regions (left) $0 < z < d_1$ and (right) $d_1 < z < d_3$ at $x = 0.75L$, when the surface-relief grating is defined by Eq. (2) and the incident plane wave is p polarized. The grating period $L = 0.8\lambda_0$ and $d_1 = 6\Omega$.

can be excited with period $L = \lambda_0$ of the surface-relief grating, the grating period needs to be changed in order to excite the remaining SPP waves. The plots of A_p vs θ for $L = 0.75\lambda_0$ are presented in Fig. 7, again for $d_1 \in \{4\Omega, 5\Omega, 6\Omega\}$. The figure shows three A_p peaks at $\theta \simeq 32.5^\circ$, 50.9°, and 64.2° that are present for all three chosen values of d_1. The relative wave numbers of several Floquet harmonics at these values of θ are given in Table IV. The A_p peak at $\theta = 32.5^\circ$ represents the excitation of a p-polarized SPP wave as a Floquet harmonic of order $n = 1$ because $k_x^{(1)}/k_0 = 1.8760$ is close to $\mathrm{Re}(1.87437 + 0.00998i)$ in Table II. The spatial profile of $P_x(0.75L,z)$ given in Fig. 8 also supports this conclusion. Similarly, the A_p peaks at $\theta = 50.9^\circ$ and 64.2° represent the excitation of two other p-polarized SPP waves as a Floquet harmonic of the same order ($n = 1$), as is evident from the comparison of Tables III and IV and from the spatial profiles of $P_x(0.75L,z)$ provided in Fig. 9.

2. $\Omega = 1.5\lambda_0$

The relative wave numbers of possible SPP waves that can be guided by the planar interface of the chosen rugate filter and the metal are given in Table V for $\Omega = 1.5\lambda_0$. In this case, the solution of the canonical boundary-value problem

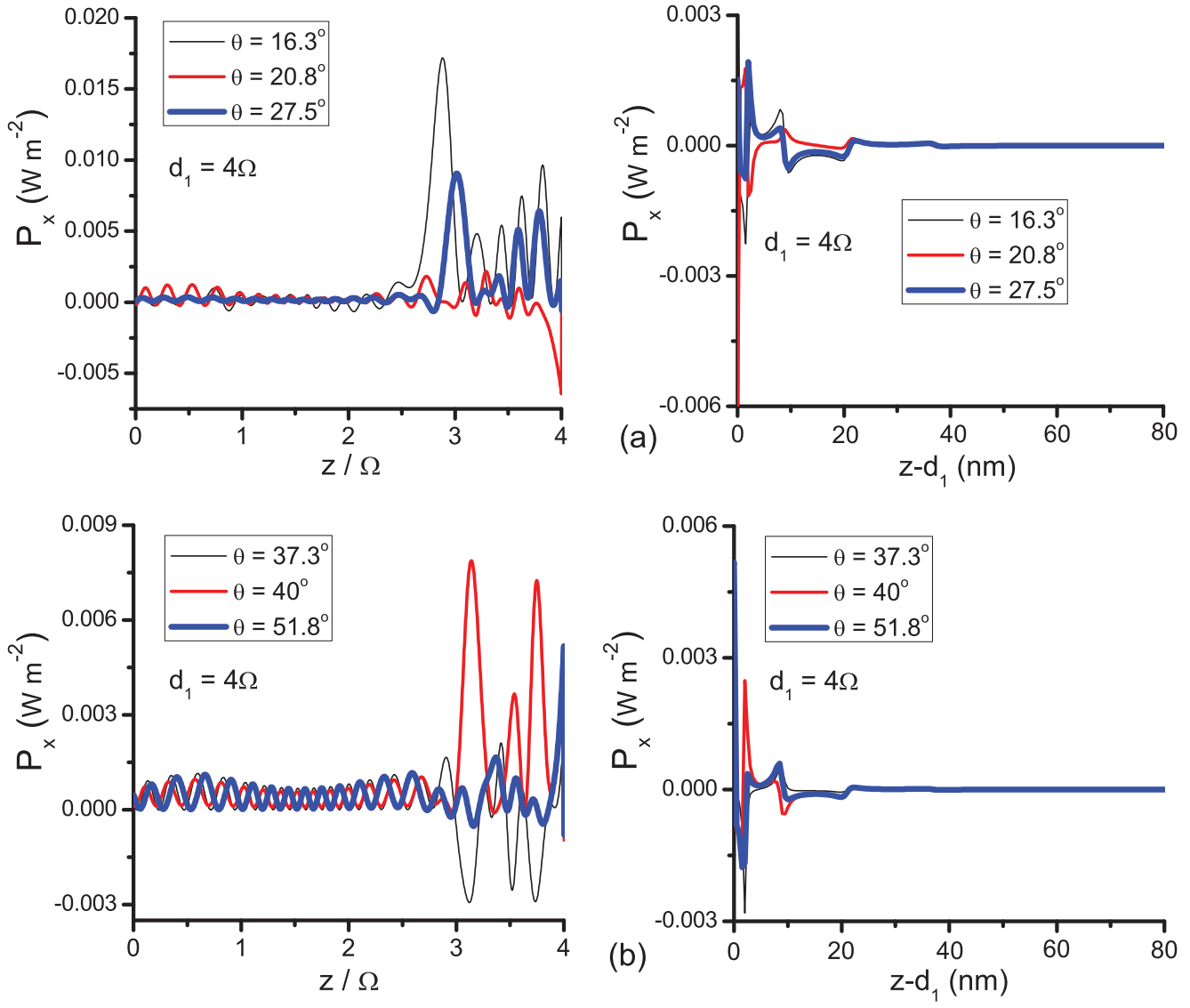

FIG. 12. (Color online) Same as Fig. 11 except that $d_1 = 4\Omega$.

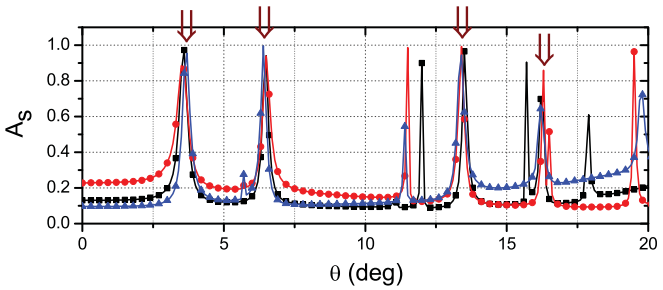

FIG. 13. (Color online) Same as Fig. 10 except that A_s is plotted instead of A_p, and $L = 0.6\lambda_0$.

[11,31] indicated that four s-polarized and six p-polarized SPP waves can be guided by the metal–rugate-filter interface. For computations, the region $d_1 < z < d_2$ was again divided into 1-nm-thick slices; however, the region $0 \leqslant z \leqslant d_1$ was divided into 3-nm-thick slices to reduce the computation time, after ascertaining that the accuracy of the computed reflectances and transmittances had not been adversely affected.

In the plots of A_p vs θ for $L = 0.8\lambda_0$, provided in Fig. 10, the excitation of p-polarized SPP waves is indicated at seven values of the incidence angle: $\theta \simeq 8.8^\circ$, 16.3°, 20.8°, 27.5°, 37.3°, 40°, and 51.8°. The relative wave numbers $k_x^{(n)}/k_0$ of a few Floquet harmonics at these values of the incidence angle are given in Table VI. The A_p peak at $\theta = 8.8^\circ$ represents the excitation of a p-polarized SPP wave because $k_x^{(1)}/k_0 = 1.4030$ is close to $\mathrm{Re}(\kappa/k_0) = 1.40725$ (Table V). The spatial profile of $P_x(0.75L,z)$ given in Fig. 11 for $\theta = 8.8^\circ$ confirms the excitation of a p-polarized SPP wave; however, the SPP wave is very loosely bound to the interface $z = d_1$ in the region $0 < z < d_1$.

The A_p peak at $\theta = 16.3^\circ$ represents the excitation of another p-polarized SPP wave, because $k_x^{(1)}/k_0 = 1.5307$ is close to $\mathrm{Re}(\kappa/k_0) = 1.54121$ (Table V). The A_p peak at $\theta = 20.8^\circ$ also represents a p-polarized SPP wave because $k_x^{(-2)}/k_0 = -2.1416$ is close to $\mathrm{Re}(\kappa/k_0) = -2.11513$ (Table V). Similarly, the A_p peak at $\theta = 27.5^\circ$ is due to the excitation of another p-polarized SPP wave as a Floquet harmonic of order $n = 1$. The spatial profiles of $P_x(0.75L,z)$ given in Fig. 12(a) for three different p-polarized plane waves incident at $\theta = 16.3^\circ$, 20.8°, and 27.5° also confirm that SPP waves are excited as Floquet harmonic of order $n = 1$, -2, and 1, respectively.

A comparison of Tables V and VI shows that the A_p peaks at $\theta = 37.3^\circ$ and 40° represent the excitation of the same p-polarized SPP wave; however, the SPP wave is excited as a Floquet harmonic of order $n = -2$ at $\theta = 37.3^\circ$ but of order

TABLE VII. Relative wave numbers $k_x^{(n)}/k_0$ of Floquet harmonics at the θ values of the peaks identified in Fig. 13 by vertical arrows when $\Omega = 1.5\lambda_0$ and $L = 0.6\lambda_0$. Boldface entries signify SPP waves.

	$n=-2$	$n=-1$	$n=0$	$n=1$	$n=2$
$\theta = 3.7^\circ$	−3.2688	**−1.6021**	0.0645	1.7312	3.3979
$\theta = 6.4^\circ$	−3.2219	−1.5552	0.1115	**1.7781**	3.4448
$\theta = 13.5^\circ$	−3.0999	**−1.4332**	0.2334	1.9001	3.5668
$\theta = 16.2^\circ$	−3.0543	−1.3877	0.2790	**1.9457**	3.6123

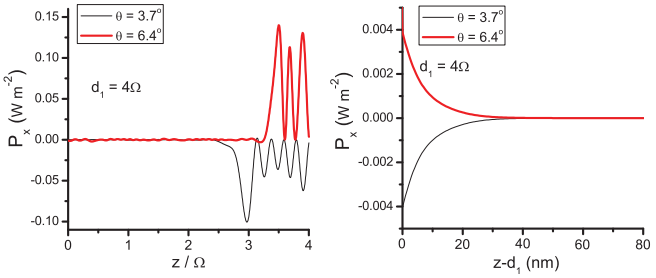

FIG. 14. (Color online) Variation of the x component of the time-averaged Poynting vector $\mathbf{P}(x,z)$ along the z axis in the regions (left) $0 < z < d_1$ and (right) $d_1 < z < d_3$ at $x = 0.75L$ for two s-polarized incident plane waves, when the surface-relief grating is defined by Eq. (2). The grating period $L = 0.6\lambda_0$, $d_1 = 4\Omega$, and $\Omega = 1.5\lambda_0$.

$n = 1$ at $\theta = 40^\circ$. Similarly, a p-polarized SPP wave is excited as a Floquet harmonic of order $n = 1$ at $\theta = 51.8^\circ$. The spatial profiles of $P_x(0.75L,z)$ given in Fig. 12(b) also support these conclusions.

In the plots of A_s vs θ for $L = 0.6\lambda_0$, provided in Fig. 13, four peaks at $\theta \simeq 3.7^\circ, 6.4^\circ, 13.5^\circ$, and 16.2° are present for all values of d_1. The A_s peak at $\theta = 3.7^\circ$ represents the excitation of an s-polarized SPP wave as a Floquet harmonic of order $n = -1$ because $k_x^{(1)}/k_0 = -1.6021$ is close to $\mathrm{Re}(\kappa/k_0) = -1.61507$ (Table V), which is a solution of the canonical boundary-value problem for an s-polarized SPP wave, whereas the A_s peak at $\theta = 6.4^\circ$ represents the excitation of another s-polarized SPP wave because $k_x^{(1)}/k_0 = 1.7781$ is close to $\mathrm{Re}(\kappa/k_0) = 1.78735$ (Table V). Similarly, two s-polarized SPP waves are excited as a Floquet harmonic of order $n = 1$ at $\theta = 13.5^\circ$ and of order $n = -1$ at $\theta = 16.2^\circ$, respectively, as is evident from the comparison of Tables VI and VII. The spatial profiles of $P_x(0.75L,z)$ given in Figs. 14 and 15 confirm these conclusions.

C. General conclusions

In the last two subsections, we have deciphered a host of numerical results and identified those absorptance peaks that indicate the excitation of SPP waves in the grating-coupled configuration, when the dielectric partnering material is periodically nonhomogeneous normal to the mean plane of the surface-relief grating. We found that

(i) the periodic nonhomogeneity of the dielectric partnering material enables the excitation of multiple SPP waves of both p- and s-polarization states;

(ii) fewer s-polarized SPP waves are excited than p-polarized SPP waves;

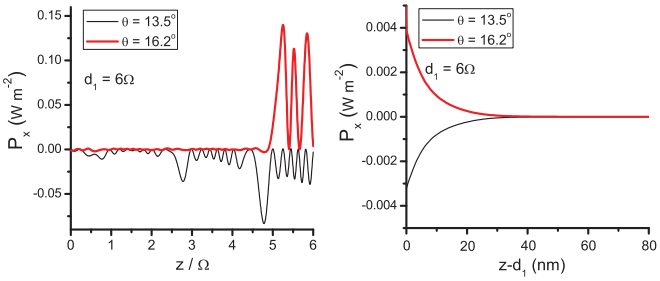

FIG. 15. (Color online) Same as Fig. 14 except that $d_1 = 6\Omega$.

(iii) for a given period of the surface-relief grating, it is possible for two plane waves with different angles of incidence to excite the same SPP wave [Figs. 4(b) and 10];

(iv) not all SPP waves predicted by the solution of the canonical problem may be excited in the grating-coupled configuration for a given period of the surface-relief grating;

(v) the absorptance peaks representing the excitation of p-polarized SPP waves are generally wider than those representing s-polarized SPP waves;

(vi) the absorptance peak is narrower for an SPP wave of higher phase speed [i.e., smaller $\mathrm{Re}(\kappa)$]; and

(vii) an SPP wave that is excited as a Floquet harmonic of order $n = +1$ for $\theta \in [0,\pi/2)$—or $n = -1$ for $\theta \in (-\pi/2,0]$, by virtue of symmetry—is the most efficient (Fig. 6).

Let us note that some other combination of the periodic functions $\epsilon_d(z)$ and $g(x)$ may allow all solutions of the canonical boundary-value problem to be excited in the grating-coupled configuration with a specific $\{d_1,d_2,d_3\}$.

The solution of the canonical boundary-value problem [11] indicates that the period 2Ω of the rugate filter needs to be greater than a certain value in order for more than one SPP wave to be excited, and the excitation of s-polarized SPP waves may require an even larger period. However, the number of possible SPP waves increases as the period increases up to a certain value.

IV. CONCLUDING REMARKS

The excitation of multiple surface plasmon-polariton (SPP) waves by a surface-relief grating formed by a metal and a dielectric material, both of finite thickness, was studied theoretically using the rigorous coupled-wave analysis for a practically implementable setup. The presence of an SPP wave was inferred by a peak in the plot of absorptance vs the angle of incidence θ, provided that the θ location of the peak turned out to be independent of the thickness of the dielectric partnering material. If that material is homogeneous, only one p-polarized SPP wave, that too of a p-polarization state, is excited. However, the periodic nonhomogeneity of the partnering dielectric material normal to the mean metal-dielectric interface results in the excitation of multiple SPP waves of different polarization states and phase speeds. In general, the absorptance peak is narrower for an s-polarized SPP wave than for of a p-polarized SPP wave, and the absorptance peak is narrower for an SPP wave of higher phase speed.

Since the electromagnetic field radiated by a line source can be considered as a spectrum of plane waves propagating at all angles [[33], Sec. 2.2], the grating-coupled configuration discussed in this paper can be used to excite multiple SPP waves simultaneously by a line source. The excitation of multiple SPP waves may be significant for practical applications—for example, to increase the absorption of light in solar cells due to the increased possibility of excitation of SPP waves [34]. This application is currently under investigation by the authors.

ACKNOWLEDGMENTS

M.F. thanks the Trustees of the Pennsylvania State University for financial assistance during his doctoral studies. A.L. thanks the Charles Godfrey Binder Endowment at the Pennsylvania State University for ongoing support of his research activities. Thanks are also due to an anonymous referee who suggested to include the spatial profiles of SPP waves.

[1] S. A. Maier, *Plasmonics: Fundamentals and Applications* (Springer, New York, 2007).
[2] *Surface Plasmon Resonance Based Sensors*, edited by J. Homola (Springer, Heidelberg, 2006).
[3] A. V. Zayats, I. I. Smolyaninov, and A. A. Maradudin, Phys. Rep. **408**, 131 (2005).
[4] M. Dragoman and D. Dragoman, Prog. Quantum Electron. **32**, 1 (2008).
[5] J. A. Polo Jr. and A. Lakhtakia, Laser Photon. Rev. **5**, 234 (2011).
[6] J. A. Polo Jr. and A. Lakhtakia, Proc. R. Soc. London A **465**, 87 (2009).
[7] M. Faryad, J. A. Polo Jr., and A. Lakhtakia, J. Nanophoton. **4**, 043505 (2010).
[8] Devender, D. P. Pulsifer, and A. Lakhtakia, Electron. Lett. **45**, 1137 (2009).
[9] T. H. Gilani, N. Dushkina, W. L. Freeman, M. Z. Numan, D. N. Talwar, and D. P. Pulsifer, Opt. Eng. **49**, 120503 (2010).
[10] A. Lakhtakia, Y.-J. Jen, and C.-F. Lin, J. Nanophoton. **3**, 033506 (2009).
[11] M. Faryad and A. Lakhtakia, J. Opt. Soc. Am. B **27**, 2218 (2010).
[12] B. G. Bovard, Appl. Opt. **32**, 5427 (1993).
[13] R. Overend, D. R. Gibson, R. Marshall, and K. Lewis, Vacuum **43**, 51 (1992).
[14] E. Lorenzo, C. J. Oton, N. E. Capuj, M. Ghulinyan, D. Navarro-Urrios, Z. Gaburro, and L. Pavesi, Phys. Stat. Sol. C **2**, 3227 (2005).
[15] C. C. Lee, C. J. Tang, and J. Y. Wu, Appl. Opt. **45**, 1333 (2006).
[16] A. Lakhtakia, J. Mod. Opt. **58**, 562 (2011).
[17] M. W. McCall and A. Lakhtakia, Electromagnetics **23**, 1 (2003).
[18] J. P. McIlroy, M. W. McCall, A. Lakhtakia, and I. J. Hodgkinson, Optik. **116**, 311 (2005).
[19] M. G. Moharam and T. K. Gaylord, J. Opt. Soc. Am. **72**, 1385 (1982).
[20] L. Li, J. Opt. Soc. Am. A **12**, 2581 (1993).
[21] M. G. Moharam, E. B. Grann, and D. A. Pommet, J. Opt. Soc. Am. A **12**, 1068 (1995).
[22] E. N. Glytsis and T. K. Gaylord, J. Opt. Soc. Am. A. **4**, 2061 (1987).
[23] F. Wang, M. W. Horn, and A. Lakhtakia, Microelectron. Eng. **71**, 34 (2004).

[24] N. Chateau and J.-P. Hugonin, J. Opt. Soc. Am. A **11**, 1321 (1994).
[25] M. A. Motyka and A. Lakhtakia, J. Nanophoton. **2**, 021910 (2008).
[26] N. S. Kapany and J. J. Burke, *Optical Waveguides* (Academic, New York, 1972).
[27] D. Marcuse, *Theory of Dielectric Optical Waveguides* (Academic, San Diego, 1991).
[28] A. Otto and W. Sohler, Opt. Commun. **3**, 254 (1971).
[29] M. Faryad and A. Lakhtakia, Phys. Rev. A **83**, 013814 (2011).
[30] P. W. Baumeister, *Optical Coating Technology* (SPIE, Bellingham, 2004).
[31] In addition to solutions provided in Fig. 1 of Ref. [11], other solutions were found. These have been identified by [a] in Tables II and V.
[32] V. A. Yakubovich and V. M. Starzhinskii, *Linear Differential Equations with Periodic Coefficients* (Wiley, New York, 1975).
[33] W. C. Chew, *Waves and Fields in Inhomogeneous Media* (IEEE Press, Piscataway, 1990).
[34] V. E. Ferry, A. Sweatlock, D. Pacifici, and H. A. Atwater, Nano Lett. **8**, 4391 (2008).